Relaxation Behavior of Polymer Blends after the Cessation of Shear

L. Kielhorn,[†] R. H. Colby,[‡] and C. C. Han*[,†]

Polymers Division, National Institute of Standards and Technology, Gaithersburg, Maryland 20899, and Department of Material Science & Engineering, The Pennsylvania State University, University Park, Pennsylvania 16802

Received August 20, 1999; Revised Manuscript Received December 15, 1999

ABSTRACT: We investigated the relaxation of a binary polybutadiene/polyisoprene blend after the cessation of steady-state shear using both in situ optical microscopy (OM) and light scattering (LS). Through fast Fourier transforms of the micrographs, we were able to directly relate our LS patterns with the real space morphology. In the steady state we observed ellipsoidal domains and strings. Upon the cessation of shear, these morphologies relaxed to the equilibrium morphology via a variety of mechanisms. After low shear rates were applied, coalescence between domains of random spatial distribution occurred. If the shear rate previously applied was sufficiently high, the strings were found to break up into small droplets forming necklace-like structures. The nonrandom spatial distribution created by shearing resulted in a long-lasting anisotropy at rest. If the previously applied shear rate was further increased, thermodynamic effects became important and anisotropies relaxed very fast as a consequence. A spinodal pattern in both real space and in the LS patterns was found to occur during the relaxation process.

I. Introduction

When polymers are blended commercially, the processing conditions usually subject these materials to complicated flows. On the other hand, the polymers are returned to the quiescent state after processing has been completed. The application of simple shear offers the possibility of modeling the behavior under flow in a more controlled environment. Monitoring the relaxation of the blend after the cessation of shear allows one to obtain insight into the kinetic processes during the approach of the final equilibrium state.[1] If a binary polymer blend is quenched into the two-phase regime, domains are formed spontaneously. In the quiescent state, the average domain structure that evolves is angularly isotropic. In a symmetric polymer blend that separates into phases of equal viscosity, a bicontinuous morphology with zero average interfacial curvature is expected. If one has a binary blend with a majority and a minority component, nearly spherical domains of the minority component embedded in a matrix filled with the majority component may be found. The application of simple shear breaks the rotational symmetry. Directional stresses are exerted on the domains, which tend to stretch the polymers and elongate the domain structure, which did not show a preferred direction at rest. These stresses increase with increasing domain size. If the stresses introduced by the shear exceed the restoring stress due to surface tension, droplets break up into smaller domains.

A simple perturbative calculation of a suspension of slightly elongated spheres was performed by Taylor.[2,3] Within his model for a fixed shear rate $\dot{\gamma}$, the domains break up if the radius R_0 of the unperturbed spherical domain exceeds a critical value $R_c \simeq \sigma/2\eta\dot{\gamma}$. Here σ is the surface tension and η is the viscosity. Because of this upper limit, shear tends to significantly narrow the domain size distribution.[4] However, shear not only introduces mechanical strains on existing domains but also changes the thermodynamic behavior. Onuki and Kawasaki[5] investigated the effect of shear on a blend undergoing spinodal decomposition. The application of shear elongates fluctuation correlations of the order parameter along the flow direction. In addition, since the application of shear introduces a new maximum time scale for fluctuations to decay, scaling assumptions allow one to introduce a new length scale k_c^{-1} related to the shear rate $\dot{\gamma}$. Fluctuations with length scales $k^{-1} > k_c^{-1}$ are suppressed in amplitude compared to their equilibrium values, whereas fluctuations with $k^{-1} < k_c^{-1}$ are little affected by the shear. Physically this means that fluctuations with long length scales, larger than k_c^{-1}, are distorted by the shear before they dissipate away thermally. Close to the critical point, the correlation length for fluctuations ξ diverges such that $k_c\xi \gg 1$ and so shear also affects the critical behavior. This regime is usually referred to as the strong shear regime. In fact, renormalization group theory predicts a shift of the critical temperature $\Delta T_c(\dot{\gamma})/T_c(0)$.[5]

$$\frac{\Delta T_c(\dot{\gamma})}{T_c(0)} = \frac{T_c(\dot{\gamma}) - T_c(0)}{T_c(0)} = -0.0832\epsilon(\tau_\xi\dot{\gamma})^{1/3\nu} \quad (1.1)$$

where $\epsilon = 4 - d$, d being the dimensionality of the system and

$$\tau_\xi = \frac{16\eta\xi_0^3}{k_B T_c} \quad (1.2)$$

is the characteristic relaxation time for the concentration fluctuations of the mixture. $\nu = 0.63$ is the usual Ising exponent for the correlation length near the critical point.[6] As the decay time of fluctuations is very long in polymeric systems owing to the connectivity of the chain, shear depression of the critical temperature is stronger than that in small-molecule systems. Another effect of the connectivity is that in the weak shear regime, where we are sufficiently far away from the critical point, such that the critical fluctuations are not

[†] National Institute of Standards and Technology.
[‡] The Pennsylvania State University.

10.1021/ma9914265 CCC: $19.00
Published on Web 03/09/2000

Table 1. Domain Structure under Steady-State Shear

number	domain structure	$\psi(\dot\gamma)/\psi(0)$
1	isotropic	1
2	elongated domains, some droplet breakup	$\simeq 1$
3	strings	<1
4	homogenized state	0

affected by the shear ($k_c\xi \ll 1$), hydrodynamic effects are suppressed, although they cannot be completely neglected.[7] Combining the thermodynamic effects with the viscoelastic effects, particularly important in entangled polymer blends, further complicates the situation as they may counteract thermodynamically induced shear mixing and actually lead to shear-induced phase separation.[8,9] In this case the decay time τ_ξ in eq 1.1 has to be replaced by the reptation time τ_{rep}. Clark and McLeish[10] recently extended previous models where the stress gradients were added as an extra driving force for the dynamics of concentration fluctuations by incorporating separate moduli and relaxation times for each of the components. As a result, shear could either induce mixing or phase separation, depending on the dimensionless ratios of the relaxation times and the moduli. Hashimoto et al.[4−7,11−21] and Han et al.[22−26] used small-angle light scattering, optical microscopy, and rheological experiments to study the behavior of polymer blend solutions under shear. In all of these experiments, a semidilute solution of polybutadiene(PB)/polystyrene-(PS) in a nonselective solvent dioctyl phthalate (DOP) using the pseudobinary approximation was investigated. Takebe and co-workers[11] found $(T_c(\dot\gamma) - T_c(0))/T_c(0) \propto \dot\gamma^{1/2}$, which agrees well with the theoretical prediction of eq 1.1. Yu et al.[22] obtained an exponent of 0.44 with a slightly higher polymer content in the solution. Using eq 1.1 and assuming[27] that $\sigma \simeq k_bT/\xi^2$, we obtain the following shear-induced reduction in the surface tension at a given temperature T

$$\sigma(\dot\gamma) \simeq \sigma(0)(1 - A(T)(\tau_\xi\dot\gamma)^{1/3\nu})^{2\nu} \qquad (1.3)$$

with $A(T) = T/(T_c(0) - T)0.0832\epsilon$ and higher terms in ϵ being neglected. If the shear rate is high enough, the surface tension is sufficiently reduced and the domains can become stringlike.[12,23] If the shear rate is further increased, the blend is eventually homogenized at a critical shear rate $\dot\gamma_c$ with

$$\dot\gamma_c = \frac{1}{\tau_\xi}\left(\frac{T_c(0) - T}{0.0832\epsilon T_c(0)}\right)^{3\nu} \qquad (1.4)$$

Even above $\dot\gamma_c$, scattering parallel to the direction of the flow is suppressed as mentioned before, since $\dot\gamma^{-1}$ represents an upper time limit for fluctuation decays. The morphology of polymer blends under shear has been categorized previously into different regimes by Hashimoto et al.,[7,16] based on the basis of analysis of the structure factor. From a morphological point of view, one can also distinguish different regimes that roughly coincide with Hashimoto's classification. The different morphologies are given in Table 1. The difference in the compositions of the phases at a given temperature T and shear rate $\dot\gamma$ in the two-phase regime is the order parameter $\psi(\dot\gamma)$ as shown in Figure 1. Hence $\psi(\dot\gamma)/\psi(0)$ is the value of the order parameter in the domains under shear normalized by the order parameter in the quiescent equilibrium state. As a consequence of shear-induced homogenization effects, this ratio will be smaller

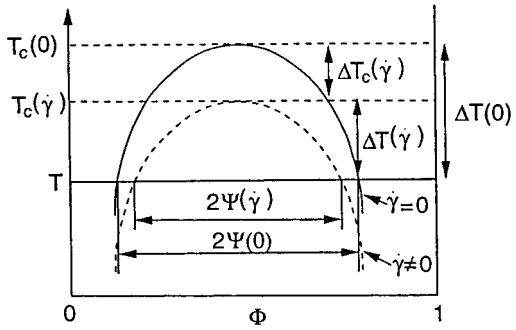

Figure 1. Effect of shear on the steady-state phase diagram of a simple binary fluid.

than one and decrease with increasing shear rate. The only difference between region I and II is that in region I the shear is so low that gravitational effects play a role. There have also been a number of studies on the relaxation behavior of the PS/PB/DOP mixture after a shear-quench. Hashimoto and co-workers investigated a quench from a shear rate of $\dot\gamma_i > \dot\gamma_c$ to the quiescent state $\dot\gamma_f = 0$.[11,13−15] Immediately after the cessation of shear a circularly symmetric scattering ring is observed. The increase in the scattering intensity was found to be consistent with the Cahn−Hilliard equation for the early stages of spinodal decomposition (SD) in a temperature quench experiment. At later times, dynamic scaling laws for the peak position $k_{max}(t)$ and the peak height $I_{max}(t)$ of the scattering function

$$k_{max}(t) \sim t^{-\alpha}$$

$$I_{max}(t) \sim t^{\beta}$$

were observed. Several distinct scaling regimes were found.[15] At intermediate times exponents of $\alpha = {}^1/_3$ and $\beta = 2$ were measured, suggesting that both the composition and the size of the domains was changing. At later stages both exponents were smaller than the values $\alpha = 1$ and $\beta = 3$, found in the late, hydrodynamically dominated, stages of temperature jump experiments. Nevertheless the exponent relation $\beta/\alpha = 3$ was fulfilled, suggesting that domain coarsening occurred without any compositional changes. Hashimoto et al. suggested that this might be due to the breakup of bicontinuous structures and the subsequent formation of a majority and a minority phase in their case of an asymmetric phase diagram. Takebe and Hashimoto[14] and Han and co-workers[24,25] also conducted shear-quench experiments starting from inhomogeneous states; i.e., the initial shear rate $\dot\gamma_i$ is below $\dot\gamma_c$. At low $\dot\gamma_i$, the anisotropy persisted for long times but the scattering pattern became diffuse as the strings disappeared and size and shape fluctuations of the domains increased. At higher shear rates, the relaxation behavior is qualitatively similar to the early stages but then an additional spinodal ring is observed. In this stage the anisotropy decays much faster. There have also been a variety of shear-quench experiments to final shear rates $\dot\gamma_f > 0$. Takebe and Hashimoto[14] quenched a system from an initial shear rate $\dot\gamma_i > \dot\gamma_c$ to low shear rates $\dot\gamma_f \ll \dot\gamma_c$. They observed the appearance of a spinodal ring in light-scattering experiments, which was then deformed by the shear flow. Moses et al.[18] monitored transient states of extremely elongated domains and reported that the viscosity changes are determined by the initial and final shear rates in the early and late states of the transition process, respectively.

All of the in situ studies conducted and mentioned so far were performed on semidilute polymer solutions where the mass fraction polymer content was between 3% and 8%. On the other hand, there have been many studies on the rheological behavior of pure polymer blends, but the number of in situ light-scattering and optical microscopy studies on pure polymer blends is very limited. In particular, relaxation studies after the cessation of steady-state shear morphologies are rare. Mewis et al.[28−35] performed a serious of shear step experiments on a blend with a small fraction (1 and 10%) of poly(dimethylsiloxane) (PDMS) in a polyisobutylene (PIB) matrix or vice versa including the cessation of shear before and after reaching a steady state using dichroism and small-angle light scattering. They found that for small deformations of the PDMS droplets, achieved by a short application of shear, regular retraction into spherical droplets occurred after the cessation of shear. If the domains had already formed highly elongated structures, the strings broke up into a smaller domains after the cessation of shear and arranged themselves in a necklace-like structure as predicted by Tomotika.[36] The different mechanisms are reflected in different light-scattering patterns. The breakup of the string into a necklace-like morphology results in the development of a secondary maximum in the flow direction, the position of which depends on the wavelength of the Raleigh instability. Mewis et al.[32] calculated the scattering patterns for an isolated cylinder with sinusoidal thickness modulations and for the necklace stucture.[31] When these were compared to their experimental data, polydispersity of the strings and interference between strings broadened experimental light-scattering patterns even at these very low droplet concentrations, but a weak secondary maximum was detected. The dimensions of the initial string and of the resulting droplets were estimated from the scattering patterns. Because of the very weak elastic properties of the blend materials, all elastic behavior was attributed to the interfacial tension, which was then estimated from the recoil process with the help of dichroism measurements. Mewis et al. also compared the relaxation behavior to several models and found quantitative agreement[29,35] in some cases. In a different set of experiments by Gronski et al., a high molecular mass polybutadiene(PB)/polyisoprene(PI) blend was sheared, but before a steady state was reached, the shear was stopped. The scattering function was found to recoil to a pattern elongated parallel to the original flow direction.[37]

Thus our paper is the first systematic study of the relaxation behavior of a pure binary polymer blend with in situ light scattering and optical microscopy. We investigated a well-defined entangled PB/PI blend in order to study the interference of thermodynamic and viscoelastic effects after the cessation of shear from a steady state. When the shear is stopped, the stress decays and at the same time the quench depth is altered as the critical temperature of the quiescent state is now in effect. The development of domains is governed by two types of effects: first, by thermodynamic effects, e.g., surface tension and quench depth, and second, by the viscoelastic behavior of the polymer. In contrast to the deformation of the droplets, which is affected by both surface tension and elasticity, coalescence is mainly a result of surface tension.

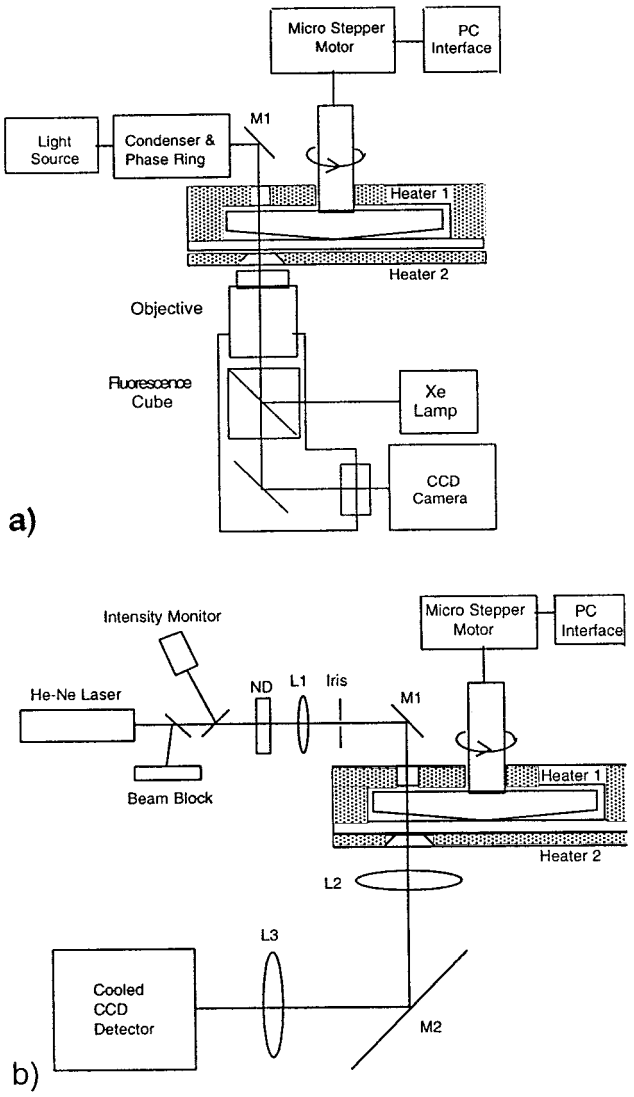

Figure 2. Schematic diagram of the shear cell. (a) shows the setup in the optical microscopy configuration; (b) shows the light-scattering configuration. ND, neutral density filters; L1, long focal length lens; L2, L3, condensers; M1,M2, mirrors.

II. Experimental Section

A. Experimental Setup. The details of the experimental setup are described elsewhere,[38] and only a brief summary will be given here. A schematic diagram of the instrument is shown in Figure 2. The heart of the instrument is the shear cell. This cell consists of two quartz plates. The top plate is connected to the motor though a milling machine, which allows precise control of the speed of revolution. Attached to the bottom plate is a heater and a thermocouple element, and both are surrounded by copper to minimize temperature gradients. The top glass plate is covered by a second copper plate into which additional heating elements and a second thermocouple element have been inserted. The whole cell is then doubly insulated against heat loss. This arrangement allows precise temperature control from ambient temperature up to 250 °C with a precision of ±0.1 °C. The instrument is set up in such a way that one can *switch from light-scattering mode to optical microscopy mode without affecting the sample cell*. The light-scattering patterns were recorded using the apparatus and a 15 mW He−Ne light source (λ = 633 nm). The laser beam is guided through a window in the top and bottom copper plates and then directed by condensers and mirrors into a cooled CCD camera. The data are acquired by a board in a PC computer for further analysis. As the difference in transmittance between the two phases is very small, phase contrast optical

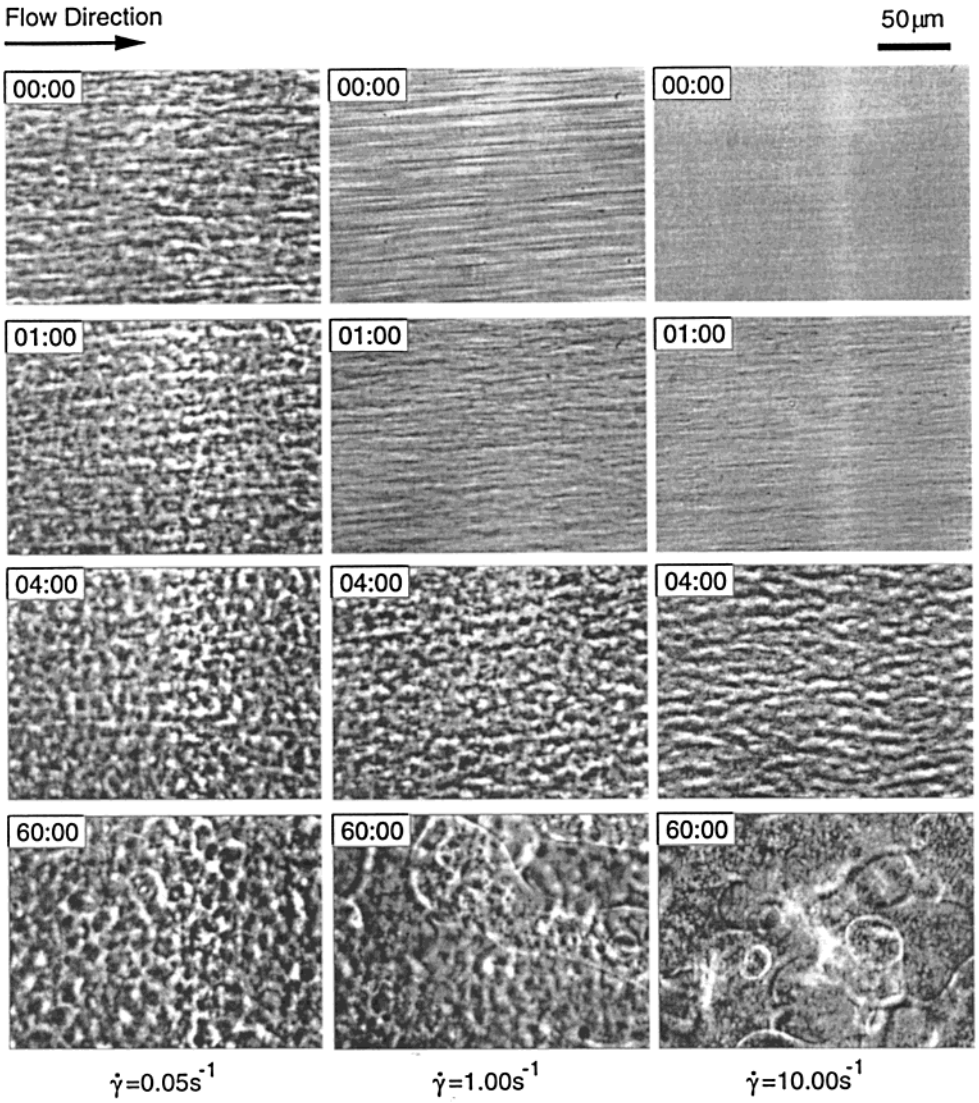

Figure 3. Optical micrographs obtained from phase contrast microscopy for shear rates of $\dot{\gamma} = 0.05\ s^{-1}$, $\dot{\gamma} = 1\ s^{-1}$, and $\dot{\gamma} = 10\ s^{-1}$ at a temperature of 110 °C. The original flow direction was horizontal. The time that has elapsed after the cessation of shear is indicated in each frame in minutes and seconds.

Table 2. Characterization Data

				microstructure,%		
sample code	polymer	M_n	M_w/M_n	1,4	1,2	3,4
LPB	PB-10	50 900	1.04	90	10	
LPI	PI-07	87 600	1.08	93		7

Table 3. Critical Conditions and Spinodal Temperatures for the Blends[a]

blend	Φ_{cr}^{PB}	χ_{cr}	χ	T_s °C
LPB/LPI	0.57	1.84×10^{-3}	$0.007\,07 - 1.75/T$	61.5

[a] The numerical values in the table are estimated to within 5%.

microscopy was used to obtain the real space images. The micrographs are acquired by another CCD camera and stored on S-VHS videotape. Fourier analysis of these images revealed that the VCR taping introduces nonphysical anisotropies. We therefore simultaneously fed these images directly to a PC and stored them with a frame grabber in order to minimize effects introduced by our data acquisition devices. Fast Fourier transformation of the micrographs can then be directly compared to light-scattering patterns.

B. Polymer Characterization. The polymers used in the experiments have been described in ref 39. The polybutadiene (PB) and polyisoprene (PI) chains used in the present experiments are random copolymers composed of 1,4- (10%), 1,2- (90%) isomers and 1,4- (7%), 3,4- (93%) isomers, respectively. The number average and mass average molecular masses[40] are given in Table 2. Presently we have only investigated the shear relaxation behavior of critical blends where the mass fraction of PB was 0.5665. The blend exhibits a lower critical temperature of 61.5 °C, which was determined in the quiescent state with cloud point measurements. Cloud point measurements were used to determine the phase separation temperatures at several compositions[41] within 1−2 °C. The critical temperature and the temperature dependence of the Flory−Huggins interaction parameter $\chi(T)$ were then obtained through a fit with the Flory−Huggins theory. The results are summarized in Table 3.

C. Sample Preparation. Appropriate amounts of LPB and LPI were dissolved in dichloromethane (net mass fraction of 2%) containing a mass fraction of 0.5% Goodyear Wingstay antioxidant.[42] The resulting mixture was stirred at room temperature for several hours until complete dissolution was observed. The solution was then ventilated with nitrogen and stirred for several more hours in order to evaporate the bulk of the solvent. The remaining solvent was finally removed in a vacuum oven at 40 °C until no more weight changes could be detected. The blend was put into the shear cell and heated to the desired temperature and sheared for at least 1 h before any data were taken. Particularly at lower shear rates, we waited considerably longer to ensure that a steady state was obtained. The shear was then stopped and the time evolution

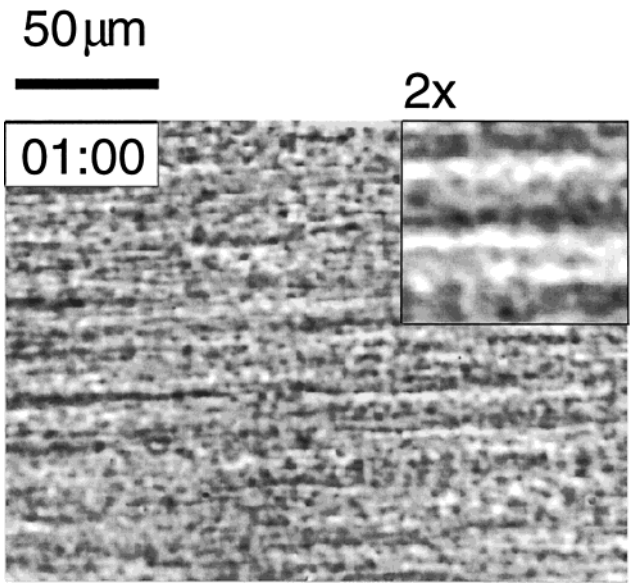

Figure 4. PCOM showing necklace-like structures 1 min after the cessation of shear due to the Raleigh instability. The original shear rate was $\dot{\gamma} = 0.1\ s^{-1}$.

of the blend was observed with light scattering and optical microscopy.

III. Results and Discussion

Figure 3 shows typical in situ micrographs of the relaxation behavior after the cessation of shear as obtained from phase contrast optical microscopy (PCOM). With a mass fraction of 0.43, PI is the minority phase and forms PI-rich domains, which are the darker areas, embedded a PB matrix. In our system phase inversion was observed at a PI mass fractions of approximately 0.55.[41] The time that has elapsed (min:s) since the shear was stopped is given in the top left corner of each frame. The left column shows the relaxation behavior after a low shear rate of $\dot{\gamma} = 0.05\ s^{-1}$ was stopped. At time $t =$ 00:00, i.e., still under shear, we can discern deformed domains, although they have lost their ellipsoidal shape. Thus we are already outside the valid range of the Taylor theory.[2,3] We have to go to shear rates below $\dot{\gamma} = 0.03\ s^{-1}$ in order to observe ellipsoidal domains for this blend. As time elapses, the deformation of the domains decreases and the domains start to coalesce. After 1 h, nearly spherical domains of PI are visible with

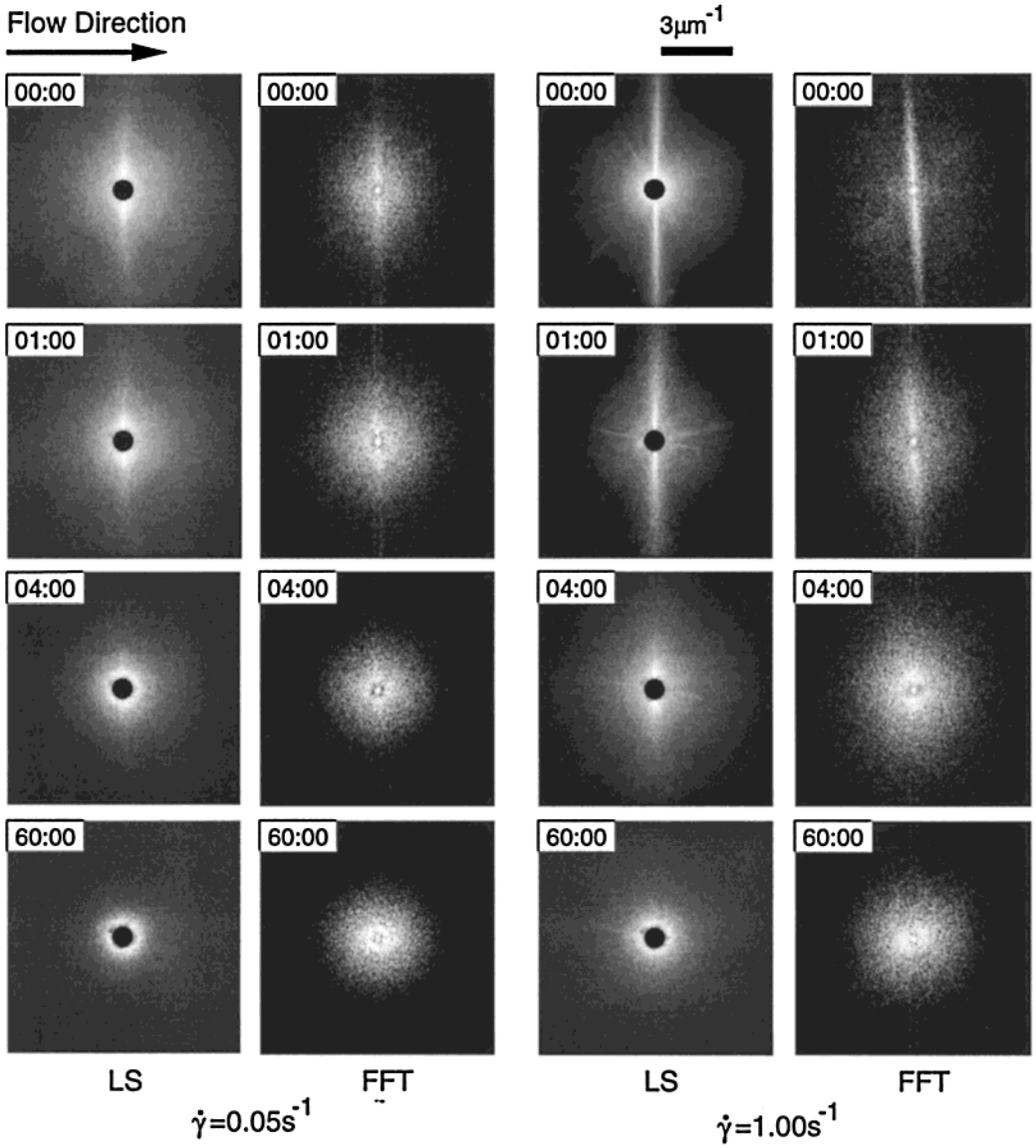

Figure 5. Comparison of scattering patterns from small-angle light-scattering with FFT images of the optical micrographs, showing that we obtain excellent qualitative agreement between the two.

a typical size of about 20 μm, but with a wide size distribution.

In the middle column, the original shear rate was 20 times higher, i.e., $\dot{\gamma} = 1\ s^{-1}$. Now a stringlike morphology develops under shear, which has been reported previously.[12,23] Upon the cessation of shear, these strings break up owing to the Raleigh[36] instability, thus creating necklace-like ordering of small domains. As the relaxation forces of the individual droplets are inversely proportional to their radius, they quickly revert to spherical shapes. After $\dot{\gamma} = 1\ s^{-1}$, the droplets are already hard to see in the micrographs. Figure 4 therefore shows an enlargement of the necklace ordering after cessation of shear with $\dot{\gamma} = 0.1\ s^{-1}$, where individual domains can clearly be seen. This nonrandom distribution has a profound effect on the relaxation behavior of the blend. Although the small broken-up domains quickly relax to spherical shapes, coalescence with neighboring domains occurs preferentially along the original flow lines. The resulting domain is therefore initially elongated in the direction of the flow. The relaxation to a spherical domain shape will become slower with each coalescence event as the resulting radius increases.

The resulting anisotropy is quite long-lived. Even after 4 min, the anisotropy due to the domain distribution is easily visible in the micrographs. Although the domains are smaller initially after the cessation of shear, the nonrandom distribution promotes domain growth. As a consequence, the domains after 1 h are larger than those observed at low shear rates (cf. the last micrograph in first column). The effect is even stronger at higher shear rates, e.g., $\dot{\gamma} = 10\ s^{-1}$, as seen in the right column in Figure 3. Under such high shear, the strings are even finer and so are the droplets immediately after the cessation of shear. After 1 h the domains, on the other hand, are much larger than those generated using lower shear rates, sometimes as big as the image area of the microscope, i.e., $\simeq$200 μm. This nonlinear response to shear perturbations of the equilibrium state has important implications. For example, strong shear mixing of the polymer during processing may not necessarily yield a more homogeneous material after the polymer has relaxed.

In addition to studying the micrographs directly, we also performed 2D fast Fourier transforms (FFT) of the micrographs. Not only does this enable us to obtain average information about anisotropies and length scales, but it also allows us to make comparisons with the in situ light-scattering (LS) experiments. Figure 5 shows both the FFT images and LS patterns for relaxation after the cessation of shear with $\dot{\gamma} = 0.05\ s^{-1}$ and $\dot{\gamma} = 1\ s^{-1}$. The agreement between the FFT and LS patterns is excellent. This combination of PCOM, FFT, and LS under the same experimental conditions allows us to directly relate real space morphologies to LS patterns, which then in turn can be used to deduce morphological information from the LS patterns obtained in other experiments. For example, we have shown that the previously reported string phase indeed has a characteristic LS streak pattern.[12,16,23,25,31,33] In addition, the FFT enables us to resolve wave vectors that are too small to be detected by our LS apparatus. At $\dot{\gamma} = 0.05\ s^{-1}$, we observe excess scattering perpendicular to the flow and suppression of scattering parallel to the flow direction.

After the shear is stopped, the scattering pattern slowly relaxes to its isotropic shape. Cuts along the 0° and the 90° axis of the LS patterns at various times after the cessation of shear are shown in Figure 6. At 0°, scattering increases at all wave vectors as time progresses, but particularly at large wave vectors. This may be consequence of the fact that after returning to a quiescent state the interface between domains can roughen as these small-scale fluctuations are no longer convected away. Also, since there is no longer an upper limit to the domain size, the domain size distribution broadens, leading to more diffuse scattering. At 90°, scattering at intermediate wave vectors decreases immediately, as extensions of the domains perpendicular to the initial flow direction can now increase drastically. About 6 min elapse before this effect affects the scattering at low wave vectors. Careful analysis of cross sections of the FFT images indicate that the typical domain size in both directions is approximately equal. After about 10 min we also observe an increase in scattering at larger wave vectors as the domain distribution broadens.

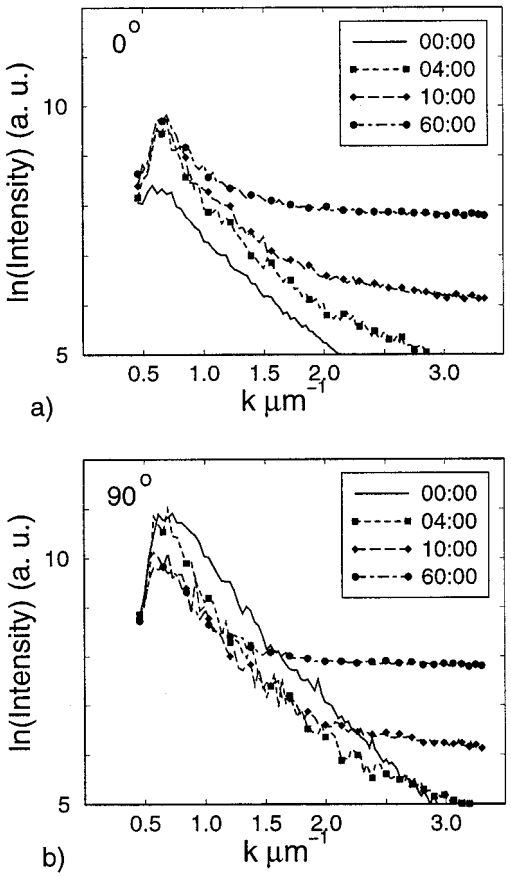

Figure 6. Time evolution of light-scattering intensities parallel (0°) and perpendicular (90°) to the original flow direction in (a) and (b), respectively. The shear rate applied before cessation was $\dot{\gamma} = 0.05\ s^{-1}$. The uncertainties are given as 1 standard deviation and are plotted in the figures as error bars only when the uncertainty limits are larger than the size of the symbol.

Figure 5 also shows the relaxation of scattering patterns after cessation of shear with $\dot{\gamma} = 1\ s^{-1}$. Under shear, most scattering parallel to the flow direction is suppressed whereas a bright streak characteristic of the string phase is visible at 90°. The anisotropy of the pattern is higher and persists longer than that observed after $\dot{\gamma} = 0.05\ s^{-1}$. The intensities parallel and perpendicular to the initial flow are shown in Figure 7. Parallel to the flow, scattering at small wave vectors increases

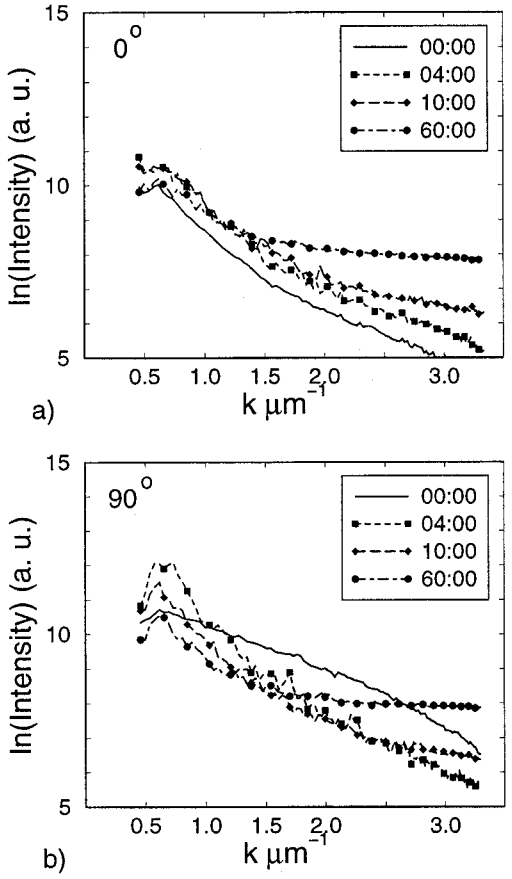

Figure 7. Time evolution of light-scattering intensities parallel (0°) and perpendicular (90°) to the original flow direction in (a) and (b), respectively. The shear rate applied before cessation was $\dot{\gamma} = 1\ s^{-1}$. The uncertainties are given as 1 standard deviation and are plotted in the figures as error bars only when the uncertainty limits are larger than the size of the symbol.

comparatively little and no distinct maximum develops in the range of wave vectors probed by our LS apparatus, implying that the extensions of any possible structural changes occurring parallel to the flow must be larger than 10 μm. At late times, scattering at large wave vectors increases. In contrast to $\dot{\gamma} = 0.05\ s^{-1}$, the scattering perpendicular to the flow increases initially at small wave vectors upon the cessation of shear. Unlike in the experiments by Mewis et al.,[32,35] no secondary maximum developed. This is not surprising because the mass fraction of PI is so high that we have polydisperse strings that constantly interfere with each other. According to Figure 1, higher shear rates lead to considerable homogenization; i.e., the compositional differences between the two phase decrease under shear. The relaxation of these compositional effects after the cessation of shear can explain the increased scattering intensities at low wave vectors in Figure 7b as we have now the increased quench depth of the quiescent state. Since the morphology evolves simultaneously, the shape of the scattering cross sections changes accordingly. We use the integrated intensities along these two axes to quantify the anisotropy $\Delta I(t)$ of the scattering patterns in the following way:

$$\Delta I(t) = \frac{\int \mathrm{d}k_{90}\, I(k,t) - \int \mathrm{d}k_0\, I(k,t)}{\int \mathrm{d}k_{90}\, I(k,t) + \int \mathrm{d}k_0\, I(k,t)} \qquad (3.5)$$

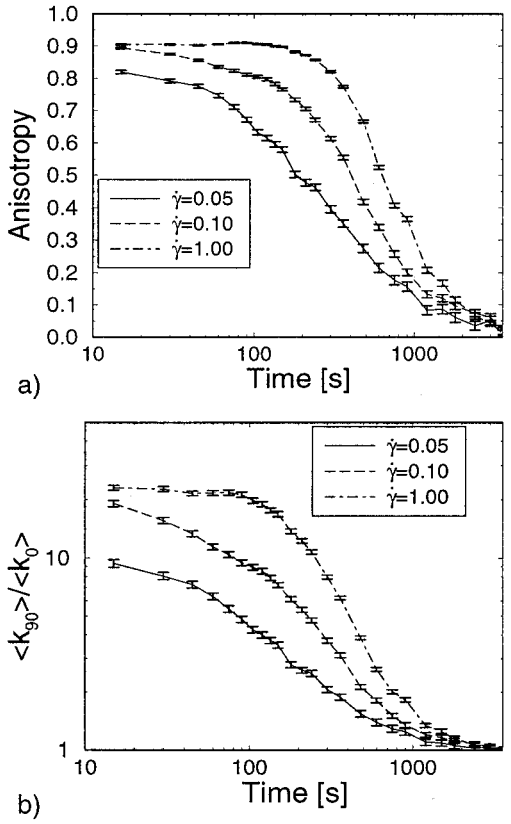

Figure 8. (a) Shear rate dependence and relaxation of anisotropy $\Delta I(t)$ at 110 °C obtained from integrated intensities as defined in the text. (b) Ratio of the first momenta of the wave vector. Error bars are the standard deviation.

$\int \mathrm{d}k_0$ and $\int \mathrm{d}k_{90}$ imply that we integrate over wave vectors parallel and perpendicular to the flow direction respectively, the other component being zero. With this definition, an isotropic scattering pattern would yield $\Delta I(t) = 0$. The relaxation of this measure of anisotropy, for the critical blend at 110 °C, is shown in Figure 8a, where, as expected, the anisotropy increases as the initial shear rate is increased and decreases with time after cessation. At higher shear rates, the anisotropy also persists longer initially but then drops faster such that after about 1000 s all scattering patterns have the same anisotropy, independent of the initial shear rate. We do not find any exponential relaxation behavior of the anisotropy. To obtain some measure of the anisotropy of typical length scales parallel and perpendicular to the original flow direction, we define an "aspect ratio" derived from the first momenta

$$\frac{\langle k_{90}\rangle}{\langle k_0\rangle} = \frac{\int \mathrm{d}k_{90}\, |k| I(k,t)}{\int \mathrm{d}k_0\, |k| I(k,t)} \qquad (3.6)$$

which is plotted in Figure 8b. The domains are highly elongated initially and more so at higher shear rates. Again, after about 1000 s, most of the relaxation has occurred regardless of the initial shear rate, and the "aspect ratio" of the domains is close to one.

Instead of using these integrated measures of anisotropy, we can study the relaxation of individual wave vectors. In Figure 9 we plotted

$$\Delta I(|k|,t) = \frac{I(k_{90}) - I(k_0)}{I(k_{90}) + I(k_0)}\Big|_{|k_{90}|=|k_0|=|k|} \qquad (3.7)$$

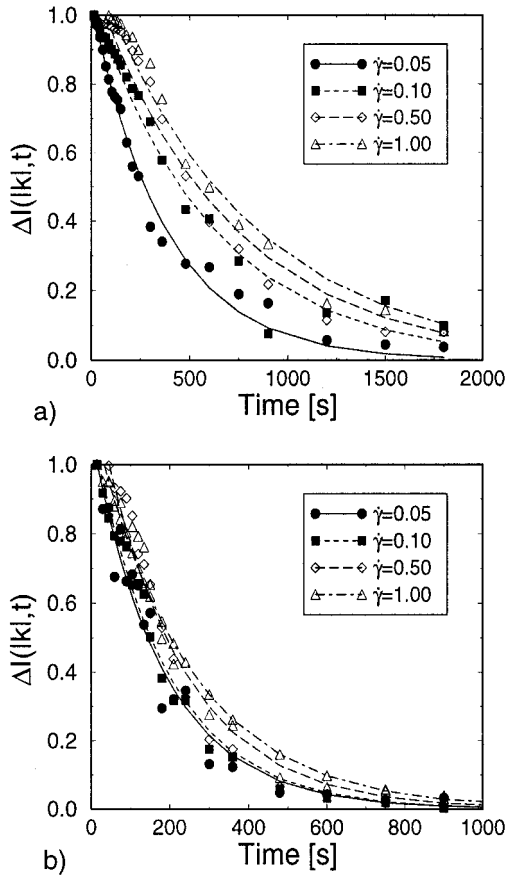

Figure 9. Relaxation behavior at wave vectors of 1 μm^{-1} in (a) and 3 μm^{-1} in (b) at 110 °C. Symbols indicate experimental data; lines indicate best fit to a simple exponential decay. At higher shear rates, compositional effects with nonexponential decay become visible at early times after the cessation of shear. The uncertainties are given as 1 standard deviation and are plotted in the figures as error bars only when the uncertainty limits are larger than the size of the symbol.

In (a) and (b) we show the relaxation of a wave vector of magnitude $|k| = 1\ \mu m^{-1}$ and $|k| = 3\ \mu m^{-1}$, respectively. One easily notices that the relaxation at the larger wave vectors occurs much faster. In addition, the dependence of the relaxation on the shear rate seems to be stronger at higher shear rates. The lines in both parts of the figure indicate a best fit assuming a simple exponential decay according to

$$\Delta I(|k|,t) = \Delta I(|k|,0)e^{-t/\tau(k)} \qquad (3.8)$$

Assuming such a simple model, we are able to extract a wave-vector-dependent characteristic relaxation time. This is summarized in Figure 10, where the relaxation time $\tau(k)$ is plotted vs $|k|$. The relaxation times decrease with increasing amplitude of the wave vector; more precisely, the relaxation times roughly decrease as $|k|^{-1}$. As a consequence, although the absolute differences in the relaxation times become smaller with increasing $|k|$, the ratio between relaxation times for different initial shear rates at any given wave vector remains nearly constant.

Describing the relaxation with an exponential decay naturally oversimplifies the situation. Close inspection of Figure 9a for $\dot{\gamma} = 1\ s^{-1}$ shows, for example, a slight nonexponential decay shortly after the cessation of shear. Deviations from simple exponential relaxation behavior for the recoil of highly elongated domains was

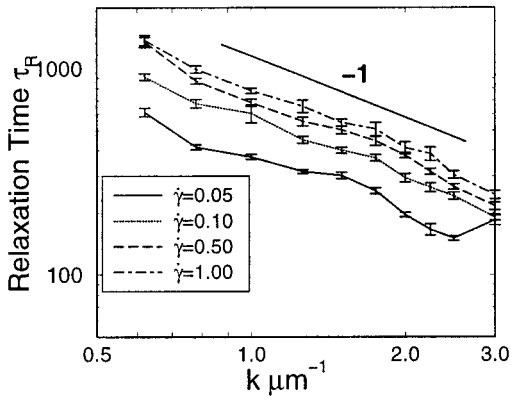

Figure 10. Wave vector dependence of relaxation time assuming a simple exponential decay for various shear rates. The relaxation times seem to be inversely proportional to the wave vector.

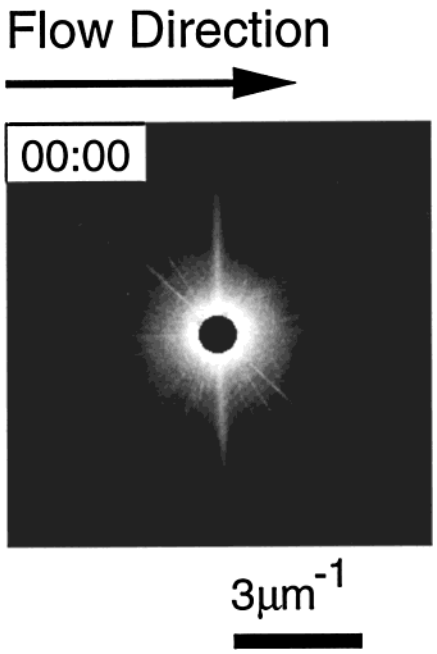

Figure 11. Light-scattering pattern under shear with $\dot{\gamma} = 50\ s^{-1}$ at 110 °C.

also reported by Van Puyvelde et al.[33] At higher shear rates and smaller wave vectors, we even observe an apparent increase in the anisotropy shortly after the cessation of shear. This effect is a consequence of the fact that shifts in composition between the two phases, owing to the difference between the steady-state compositions under shear, $\psi(\dot{\gamma})$, and the equilibrium compositions in the quiescent state after the cessation of shear, $\psi(0)$, contribute to changes in scattering in a nontrivial fashion (cf Figure 1).

We have also studied the relaxation when higher initial shear rates were used. As the fluid does not come to rest immediately after the cessation of shear, owing to inertia effects, and since degradation might start to play a role, albeit small, we present these data separately. We do not expect any of these effects to change the qualitative behavior significantly. At a shear rate of $\dot{\gamma} = 50\ s^{-1}$, homogenization effects are strong but we still have two phases with a string morphology as the weak streak at 90° in the LS pattern in Figure 11 shows. The optical micrographs, their FFT, and the LS patterns after the cessation of shear with $\dot{\gamma} = 50\ s^{-1}$ are shown in Figure 12. From the OM we conclude that the

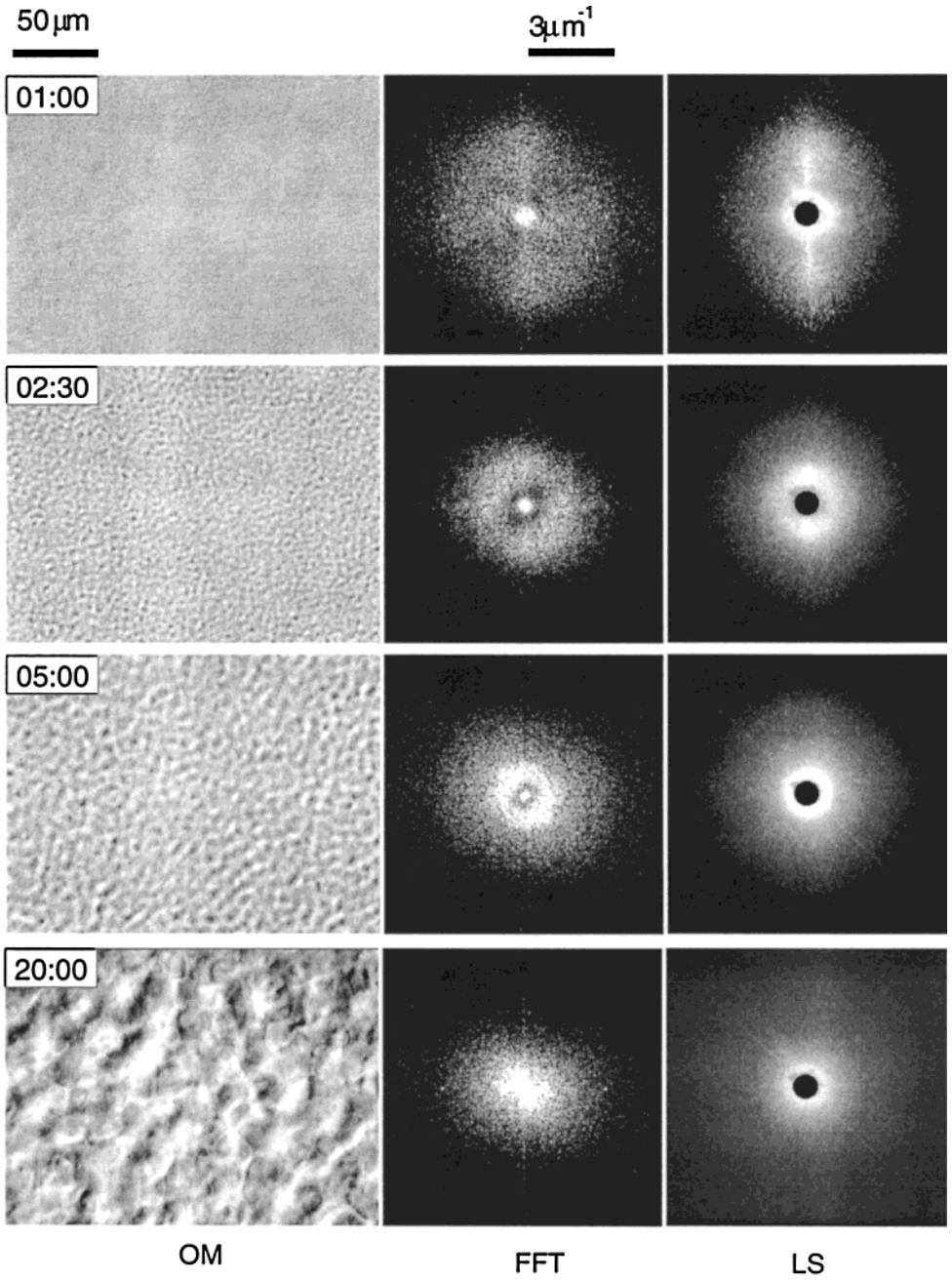

Figure 12. Relaxation after an applied shear rate of $\dot{\gamma} = 50\ s^{-1}$ at 110 °C. Spinodal patterns become visible with in 2 min. The characteristic wave vector is soon too small to be detected by light scattering, but evidence of the characteristic length scale is clearly visible in the FFT patterns.

necklace structure of the droplets due to the Raleigh instability breaks up immediately. Consequently, both the FFT patterns and the LS patterns show a relatively small anisotropy when compared to the corresponding patterns at lower shear rates (e.g., $\dot{\gamma} = 1\ s^{-1}$ in Figure 5). Within 2 min we observe spinodal structures typically found in temperature quench experiments. The patterns in reciprocal space, accordingly, show a ring and are virtually isotropic. Spinodal rings in LS patterns in semidilute polymer mixtures after shear quenches from two-phase have been observed previously[14,24] but have not been confirmed in true binary blends. Also no confirmation in real space of bicontinuous spinodal structures from in situ optical microscopy has been given up to now. The appearance of the thermodynamic effect is easily understood if the large difference between the apparent quench depth under high steady-state shear $\Delta T(\dot{\gamma})$ and the quench depth in the quiescent state $\Delta T(0)$ is considered as described in Figure 1. These spinodal structures coarsen as time progresses until the asymmetry in the blend forces the formation of a minority and a matrix phase. Unfortunately the spinodal ring moves behind the beam stop within 3−4 min, and we have to rely solely on the FFT patterns to follow the domain growth.

The time evolution of the spherically averaged structure factor as obtained from the FFT images is shown in Figure 13. The intensities were multiplied by an arbitrary factor to avoid overlap. The shift of the peak to smaller wave vectors, expected from domain coarsening, is clearly visible. We also plotted the peak position in reciprocal space vs time in Figure 14. Our data suggest power law growth where the typical domain size $R(t)$ scales as t^{α} with exponent $\alpha = 0.84$ after an

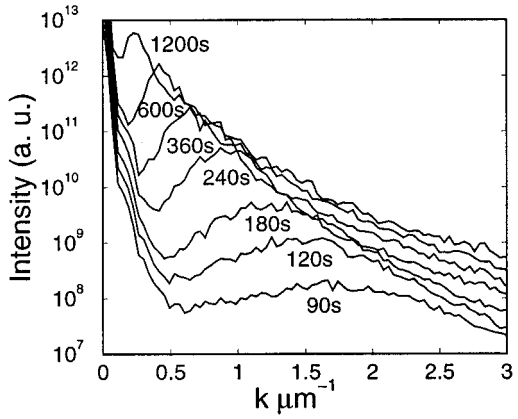

Figure 13. Spherically averaged structure factor obtained from the FFT patterns. Each curve has an offset to avoid overlap.

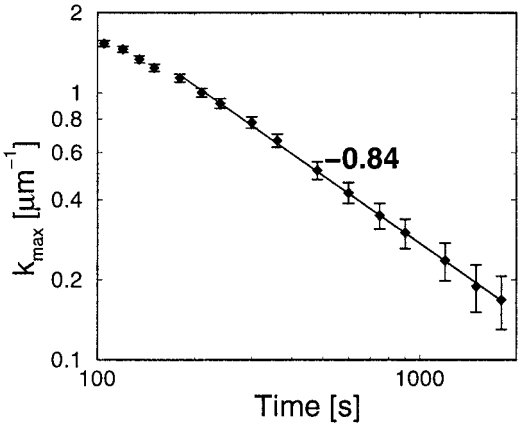

Figure 14. Time dependence of the wave vector at the maximum. The straight line is a fit to $k(t) \sim t^{-\alpha}$, with $\alpha = 0.84$

induction time of about 2 min. According to the Lifshitz−Slyozov law,[43] an exponent of $\alpha = {}^1/_3$ should be observed whereas hydrodynamic considerations should yield $\alpha = 1$. The exponent we observe is relatively close to the $\alpha = 1$, suggesting that hydrodynamic effects are important at long times. The deviation from $\alpha = 1$ might be due to the fact that at late times bicontinuous structures must evolve into isolated domains of the minority component (PI) in a matrix of the majority component (PB). Nevertheless, the fact that we observe a power law indicates that our system at that time is characterized by one length scale, $R(t)$, for some time.

There is, however, one question that deserves further investigation in the future: how does the blend get from a string phase under shear to the bicontinuous structure during relaxation? There are several possible paths one could imagine. The micrographs suggest that the strings break up into small droplets, as was the case at lower shear rates, but that the necklace-like domain distribution vanishes quickly. These droplets might adjust their composition and start to grow irregularly, eventually forming bicontinuous structures as they connect to their neighbors. It is also conceivable that phase separation occurs within the droplets themselves as the differences in composition under steady-state shear and in the quiescent state are large. In this case the minority phase within the droplets and the majority phase of the surrounding matrix, having the same composition, may merge, thus forming rugged, irregular domain shapes. And finally one could imagine that the initial droplet

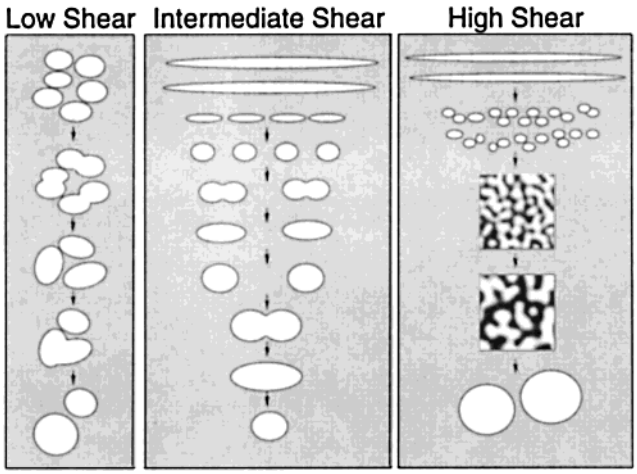

Figure 15. Schematic diagram of the different types of relaxation behaviof of a polymeric blend after the cessation of shear.

size is below the critical radius for these domains to grow. In this case the droplets would disappear, and consequently domains on the size of the spinodal wavelength would reappear. The critical radius of a spherical domain above which the nucleus will grow is dictated by the competition of the surface energy σ and the bulk energy ϵ and is given by $R_c = 2\sigma/\epsilon$. A rough estimate of this number yields $R_c \simeq 0.12$ μm. An approximate value for $\sigma = 0.17 \times 10^{-3}$ N/m was obtained from the Taylor theory,[41] and for $\epsilon = 2781$ J/m^3 was calculated with the Flory−Huggins interaction parameter at the critical composition at 110 °C. $R_c \simeq 0.12$ μm is at the lower end of our resolution and only a rough estimate, but the micrographs suggest that the domains after shear breakup are still bigger than the critical radius. Nevertheless, further measurements are needed to investigate the exact mechanism of domain evolution during the early stages after the cessation of shear.

IV. Conclusions

In this study we investigated the relaxation of a binary polymer blend after the cessation of shear with optical microscopy and light scattering. The relaxation behavior was found to be rich with interesting physics. Several effects play significant roles. A schematic summary is given in Figure 15. At low shear rates, spherical domains are deformed to ellipsoids and very large domains break up according to the Taylor theory. At these low shear rates, the domain distribution is more or less random. After the cessation of shear, the domains relax their shape and coalesce. As the domain deformation itself is relatively small and there is no preferred direction of coalescence, the anisotropy decays rapidly. At higher shear rates, stringlike domains are formed under shear. After the cessation of shear, these domains break up into small droplets, which relax into spherical shapes relatively quickly owing to the strong effect of the surface tension. The domains themselves are arranged in a necklace-like structure. This nonrandom distribution in turn makes coalescence along the original streamlines more likely. Thus anisotropies are created that last over a long time as both the deformation of the domain and the distribution of domains retain a preferred direction along the original shear direction. At even higher shear rates, we still observe a string phase and homogenization effects are now very

important. Upon cessation of shear, spinodal patterns appear after a certain induction time. These patterns are similar to those observed in temperature quenches. How the system evolves from the string phase and the subsequent formation of droplets to these patterns is unclear at present. Owing to the asymmetry in our blend, the domains coarsen over time with a power law growth, until the bicontinuous structure vanishes. The various mechanisms, of course, can never be separated as clearly as depicted in Figure 15, as a combination of all of them always comes into play at any given shear rate. Nevertheless at some shear rates one effect seems to dominate over the other two.

Acknowledgment. L.K. thanks H. S. Jeon for his help and useful discussions, in particular for the measurements that helped us with the interpretion of some of our data. We acknowledge Yvonne A. Akpalu for her assistance in preparing the manuscript and for the helpful discussions.

References and Notes

(1) For a comprehensive review, see: Onuki, A. *J. Phys.: Condens. Matter* **1997**, *9*, 6119.
(2) Taylor, G. I. *Proc. R. Soc. London, Ser. A* **1932**, *138*, 41.
(3) Taylor, G. I. *Proc. R. Soc. London, Ser. A* **1932**, *146*, 501.
(4) Hashimoto, T.; Matsuzaka, K.; Fujioka, K. *J. Chem. Phys.* **1998**, *108*, 6963.
(5) Onuki, A.; Kawasaki, K. *Ann. Phys.* **1979**, *121*, 456.
(6) Zinn-Justin, J. In *Quantum Field Theory and Critical Phenomena*; Clarendon: Oxford, 1989.
(7) Hashimoto, T.; Takebe, T.; Suehiro, S. *J. Chem. Phys.* **1988**, *88*, 5874.
(8) Onuki, A. *J. Phys. Soc. Jpn.* **1990**, *59*, 3427.
(9) Milner, S. T. *Phys. Rev. E* **1993**, *48*, 3674.
(10) Clark, N.; McLeish, T. C. B. *Phys. Rev. E* **1993**, *48*, 3674.
(11) Takebe, T.; Sawaoka, R.; Hasimoto, T. *J. Chem. Phys.* **1989**, *91*, 4369.
(12) Hashimoto, T.; Matsuzaka, K.; Moses, E. *Phys. Rev. Lett.* **1995**, *74*, 126.
(13) Takebe, T.; Hasimoto, T. *Polym. Commun.* **1988**, *29*, 227.
(14) Takebe, T.; Hasimoto, T. *Polym. Commun.* **1988**, *29*, 261.
(15) Hashimoto, T.; Takebe, T.; Asakawa, K. *Physica A* **1993**, *194*, 338.
(16) Takebe, T.; Fujioka, K.; Sawaoka, R.; Hasimoto, T. *J. Chem. Phys.* **1990**, *93*, 5271.
(17) Hashimoto, T.; Fujioka, K. *J. Phys. Soc. Jpn.* **1990**, *60*, 356.
(18) Moses, E.; Kume, T.; Hashimoto, T. *Phys. Rev. Lett.* **1994**, *72*, 2037.
(19) Fujioka, K.; Takebe, T.; Hasimoto, T. *J. Chem. Phys.* **1993**, *98*, 717.
(20) Matsuzaka, K.; Koga, T.; Hashimoto, T. *Phys. Rev. Lett.* **1998**, *80*, 5441.
(21) Kume, T.; Hattori, T.; Hasimoto, T. *Macromolecules* **1997**, *30*, 427.
(22) Yu, J.-W.; Douglas, J. F.; Hobbie, E. K.; Kim, S.; Han C. C. *Phys. Rev. Lett.* **1997**, *78*, 2664.
(23) Hobbie, E. K.; Kim, S.; Han, C. C. *Phys. Rev. E* **1996**, *54*, R5909.
(24) Nakatani, A. I.; Han, C. C. In *Structure and Properties of Multiphasic Polymeric Materials*; Araki, T., Qui, T.-C., Shibayama, M., Eds.; Marcel Dekker: New York, 1998.
(25) Kim, S.; Hobbie, E. K.; Yu, J.-W.; Han C. C. *Macromolecules* **1997**, *30*, 8245.
(26) Hobbie, E. K.; Hair, D. W.; Nakatani, A. I.; Han C. C. *Phys. Rev. Lett.* **1992**, *69*, 1951.
(27) Moldover, M. R. *Phys. Rev. A* **1985**, *31*, 1022.
(28) Vinckier, I.; Mewis, J.; Moldenaers, P. *Rheol. Acta* **1999**, *38*, 198.
(29) Vinckier, I.; Mewis, J.; Moldenaers, P. *Rheol. Acta* **1999**, *38*, 65.
(30) Minale, M.; Moldenaers, P.; Mewis, J. *J. Rheol* **1999**, *43*, 815.
(31) Yang, H.; Zhang, H.-J.; Moldenaers, P.; Mewis, J. *Polymer* **1998**, *39*, 5731.
(32) Mewis, J.; Yang, H.; Van Puyvelde, P.; Moldenaers, P.; Walker, L. M. *Chem. Eng. Sci.* **1998**, *53*, 2231.
(33) Van Puyvelde, P.; Yang, H.; Moldenaers, P.; Mewis, J. *J. Colloid. Interface Sci.* **1998**, *200*, 86.
(34) Vinckier, I.; Moldenaers, P.; Mewis, J. *J. Rheol.* **1997**, *41*, 705.
(35) Vinckier, I.; Mewis, J.; Moldenaers, P. *Rheol. Acta* **1997**, *36*, 513.
(36) Tomotika, S. *Proc. R. Soc. London, Ser. A* **1935**, *150*, 322.
(37) Gronski, W.; Läuger, J.; Laubner, C. *J. Mol. Struct.* **1996**, *383*, 23.
(38) Kim, S.; Yu, J.-W.; Han, C. C. *Rev. Sci. Instrum.* **1996**, *67*, 3940.
(39) Thudium, R. N.; Han, C. C. *Macromolecules* **1996**, *29*, 2143.
(40) According to ISO 31−8, the term "Molecular Weight" has been replaced by "Relative Molecular Mass", symbol M_r. Thus, if this nomenclature and notation were to be followed in this publication, one would write $M_{r,n}$ instead of the historically conventional M_n for the number average molecular weight, with similar changes for M_w, M_z, and M_v, and it would be called the "Number Average Relative Molecular Mass". The conventional notation, rather that the ISO notation, has been employed for this publication.
(41) Jeon, H. S.; Nakatani, A. I.; Han, C. C, in preparation.
(42) Certain equipment and instruments or materials are identified in the paper in order to adequately specify the experimental details. Such identification does not imply recommendation by the National Institute of Standards and Technology, nor does it imply the materials are necessarily the best available for the purpose.
(43) Lifshitz, I. M.; Slyozov, V. V. *J. Phys. Chem. Solids* **1961**, *19*, 35.

MA9914265